

High-Throughput Aging System for Parallel Maximum Power Point Tracking of Perovskite Solar Cells

Hans Köbler, Sebastian Neubert, Marko Jankovec, Boštjan Glažar, Martin Haase, Clemens Hilbert, Marko Topič, Bernd Rech, and Antonio Abate*

In this research instrument article, the capabilities and details of a high-throughput aging system for parallel maximum power point tracking (MPPT) of perovskite solar cells (PSCs), capable of assessing the operational stability of a large number of devices, are presented. The intention is to provide insights into the machine and the development process to engineers who want to create a similar system and eventually make MPPT stability testing of PSCs a standard procedure.

1. Introduction

The power conversion efficiency (PCE) of perovskite solar cells (PSCs) has significantly improved over the past decade.^[1] A major challenge remaining to be solved for the technology to become commercialized is the low operational stability. It is known that, for example, water, oxygen, and UV-light are harmful to PSCs,^[2–4] but these issues are likely to be solved on a technical level by proper encapsulation^[5–7] or UV-filters.^[8,9] However, some stressors are intrinsic to the operation of a solar

cell, like non-UV light, the photovoltage of the cell, and the temperature during operation. This makes it worth testing and evaluating the operational stability of PSCs.

The high-throughput aging system was built in 2018 in cooperation among Helmholtz-Zentrum Berlin, the LSA GmbH, and the Laboratory of Photovoltaics and Optoelectronics from the University of Ljubljana and has been constantly tested and improved since then.

The aging system is able to simultaneously perform continuous maximum power point tracking (MPPT) of 384 individual solar cells. To the best of our knowledge, this is the setup with the highest measurement capacities in one machine existent. The setup is furthermore capable of precisely controlling the substrate temperature to be constant or cycled, provides sample chambers with atmospheric control, and has the option to perform dark-light cycling. Table 2 gives an overview of the essential features of the system.

The system has already proven to be a powerful tool to test PSCs in controlled conditions and enables us to run different ISOS-protocols.^[10] Table S1, Supporting Information, gives all publications to date^[11–23] that involve measurements done on the system along with the used ISOS protocol. Table 1 shows the most used ISOS protocols on the presented aging setup. Table S2, Supporting Information, gives a complete overview of all measurement conditions that can be performed.

It has been found that excess charge carriers remaining in the solar cell induce phase instability of the perovskite material. Excess charges promote the migration of ions in the material by lowering the activation energy for the migration, which leads to phase segregation.^[24] In the open-circuit condition, excess charges are accumulated in the device. This is likely one reason why aging results strongly differ depending on the bias condition during the aging.^[25] Another study found that also in light-cycling experiments, both the photodegradation and the following recovery processes are heavily influenced by the electrical bias condition during aging.^[26] Consequently, while it is not exclusively a feature of perovskite solar cells,^[27] it is essential for this young technology to age the solar cells in the MPPT mode and not in the easy to access yet unrealistic open-circuit condition. Other load conditions may also introduce degradation paths that don't exist in MPPT mode, and it is unknown how the results translate from one condition to the other. Additionally, since the real-world operation is generally performed at maximum power point (MPP), we highly recommend to age PSCs in this load condition. Therefore, this machine is designed to test


H. Köbler, A. Abate
Department Novel Materials and Interfaces for Photovoltaic Solar Cells
Helmholtz-Zentrum Berlin für Materialien und Energie
Kekuléstraße 5, 12489 Berlin, Germany
E-mail: antonio.abate@helmholtz-berlin.de

S. Neubert, M. Haase, C. Hilbert
LSA GmbH
Äußerer Hofring 11, 09429 Wolkenstein, Germany

M. Jankovec, B. Glažar, M. Topič
Laboratory of Photovoltaics and Optoelectronics
Faculty of Electrical Engineering
University of Ljubljana
Tržaška cesta 25, SI-1000 Ljubljana, Slovenia

B. Rech
Helmholtz-Zentrum Berlin für Materialien und Energie
Hahn-Meitner-Platz 1, 14109 Berlin, Germany

B. Rech
Faculty of Electrical Engineering and Computer Science
Technische Universität Berlin
Marchstraße 23, 10587 Berlin, Germany

 The ORCID identification number(s) for the author(s) of this article can be found under <https://doi.org/10.1002/ente.202200234>.

© 2022 The Authors. Energy Technology published by Wiley-VCH GmbH. This is an open access article under the terms of the Creative Commons Attribution License, which permits use, distribution and reproduction in any medium, provided the original work is properly cited.

DOI: 10.1002/ente.202200234

Table 1. Most commonly used ISOS^[10] aging protocols in the presented aging system.

ISOS-protocol	Light condition	Temperature	Atmosphere	Load ^{a)}
ISOS-L-1I	Constant	25 °C	Nitrogen	MPPT
ISOS-L-2I	Constant	65, 85 °C	Nitrogen	MPPT
ISOS-LC-1I	Cycled	25 °C	Nitrogen	MPPT
ISOS-LC-2I	Cycled	65, 85 °C	Nitrogen	MPPT
Thermal cycling under operation ^{b)}	Constant	cycled	Nitrogen	MPPT

^{a)}While the ISOS protocols also allow for OC condition, we would like to highlight the necessity for aging with MPPT here. ^{b)}Not defined as ISOS protocol.

perovskite solar cells in MPP conditions. This is technologically challenging since it requires electronics that track the MPP of each solar cell. We specifically designed measurement electronics for this purpose, and details are given in Section 3.

While the efficiencies of PSCs have sky-rocketed to values^[1] close to the Shockley–Queisser limit,^[28,29] the reproducibility of PSCs is still low.^[30] Therefore, this high-throughput system allows us to test many solar cells in parallel and thus to provide statistics allowing for robust statements.

2. System Description

Figure 1 shows the complete system, which has the dimensions of $1.3 \times 0.8 \times 2 \text{ m}^3$, and a schematic of the subsystems.

The system is controlled by a programmable logic controller (PLC) and accessed via a graphical user interface (GUI) on a windows computer. The software is custom-made by the LSA GmbH. On-the-fly data is stored in a Microsoft SQL database, output as an Excel document, and then processed with MATLAB scripts according to the needs of the analysis.

An integral part of the system are the sample boxes (a). They are built air-tight and are constantly flushed with nitrogen and therefore provide atmospheric control (b), which is particularly important for PSCs.^[31] Currently, the system can host eight such sample boxes, and each box can host eight devices carrying six solar cells. Therefore, 384 individual solar cells can be measured in parallel. The advantage of a modular system is that different aging conditions can be applied to every box. Thus, various experiments can be run in parallel. For example, the sample temperature and the electronic load conditions can be varied, but also light cycling can be applied to a specific box. Another advantage of a modular system is that the other part-systems can still be operated when maintenance is necessary on one of the sample boxes. Also, the volume that needs to be nitrogen-controlled is reduced, for example, compared to a system entirely fitted into a glovebox. Our high-throughput ageing setup also provides a secondary gas feeding system, which can be attached to another type of gas like dry air or air. With the flick of a switch, the atmosphere in a sample box can be changed. The use of humid air is not intended in this particular setup due to possible corrosion of parts.

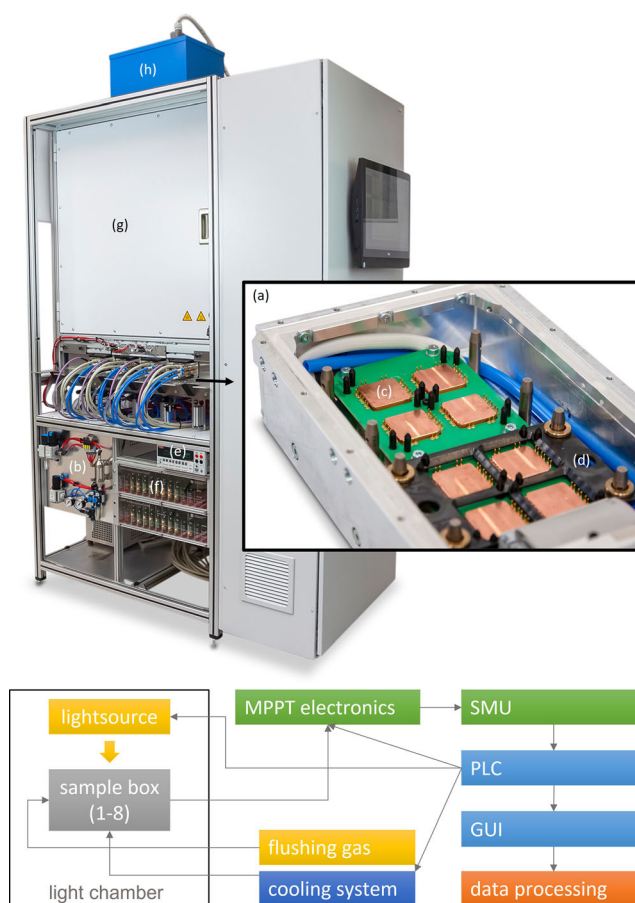


Figure 1. The high-throughput aging system and schematic of the subsystems.

We are aware that in an open system, the nitrogen flow may remove degradation products from the cells which can possibly prevent a back reaction and therefore influence the aging behavior.^[32] However, this will largely depend on the dominant degradation pathway which is also influenced by the applied temperature. Therefore, we cross-check aging results with encapsulated devices on a regular basis, while the intention of high-throughput screening is better matched with unencapsulated devices.

The sample boxes contain a contacting system (c). Our in-house solar cell device layout is shown in Figure S1, Supporting Information. A device carries six solar cells, and three of the solar cells share a common ground, the so-called busbar. Thus, a device features eight contacts. The cells are contacted in a four-wire setup with two pins per contact, and the contacting is realized with spring-loaded gold pins attached to a custom-made printed circuit board (PCB). A PCB is an elegant way to fit many connections into the limited space of a box. A sample box is then attached to the measurement electronics via small computer system interface (SCSI) cables. The samples are held down onto the contacting and thermal coupling by a fixation plate (d) which is screwed down. The measurement electronics can route a single solar cell to a source measure unit (SMU) (e) to perform sequential current density – voltage scans (J – V scans) on every solar cell.

Another central part of the system is the custom-made MPPT electronics (f) made by the Laboratory of Photovoltaics and Optoelectronics. We dedicated the next chapter to electronics for details. The measurement electronics allow for different testing modes: MPPT, short-circuit, open-circuit, and constant voltage. The system is passive, meaning that no voltage is applied. Instead, the load resistance of a solar cell is varied. Consequently, in constant voltage mode, the voltage can only be set to a value between 0 V and V_{oc} .

Samples are actively temperature controlled by thermoelectric heat pumps (Peltier elements). Two Peltier elements control the temperature of the eight samples of one box. The Peltier elements are connected in parallel and are sourced by a single DC power supply for each box. This is advantageous over a pulse-width-controlled power supply due to an improved lifetime of the Peltier elements and improved electromagnetic compatibility. The Peltier elements' driving voltage and polarity (heating/cooling) is controlled by the PLC via a closed feedback loop incorporating PT100 sensors sitting in the copper blocks above the Peltier elements. The temperature can be constant or cycled; the temperature range is -10 to 100 °C. The Peltier elements are thermally coupled to a cooling circuit, providing tempered water for all the boxes. On top of the elements, there is a copper block (c) which serves as a sample stage. On top of the copper, there is a pad attached that consists of thermal interface material and is topped by glass-polytetrafluoroethylene (PTFE) tape (shown in Figure 10). This material combination serves multiple purposes: It is thermally conductive to connect the samples to the Peltier heat control, electrically insulating to not connect the single solar cells on one substrate, chemically inert to avoid introducing interactions with the cells, nonsticky in order not to damage samples when they are released from the system and also soft to serve as elastic bearing and not to damage samples by the applied hold-down pressure. The active surface of the solar cells is directly attached to the PTFE surface.

To perform an experiment, the sample boxes are slid into a big light chamber (g). The light source (h) is a Hoenle SOL 2000 metal halide lamp with an H6 spectrum shaping filter. The system actively controls the metal halide lamp via a global monitoring cell to maintain the desired illumination intensity. As a UV filter, the UV-blocking foil "KFU15" by Mitsui is optionally used to block UV-light with wavelengths below 380 nm. The spectrum of the lamp with and without UV filter compared to the AM1.5 G spectrum is shown in Figure 2.

Dark-light cycles can be run on two sample boxes with the help of a shutter system (see Figure S2, Supporting Information), which shades an entire box. The duration of the illuminated and the dark phase can be controlled. When cells are in the dark, they are put to open-circuit conditions automatically. The shutter system gives access to the ISOS-LC and ISOS-LT protocols,^[10] thus allowing to perform studies on the day-night behavior, which is unusual for PSCs.^[33–35] During the dark phase, sequential J – V scans in dark and light conditions or short MPPT in light can be performed in a defined interval to inquire about recovery times.

Table 2 gives an overview of the essential properties of the high-throughput aging system.

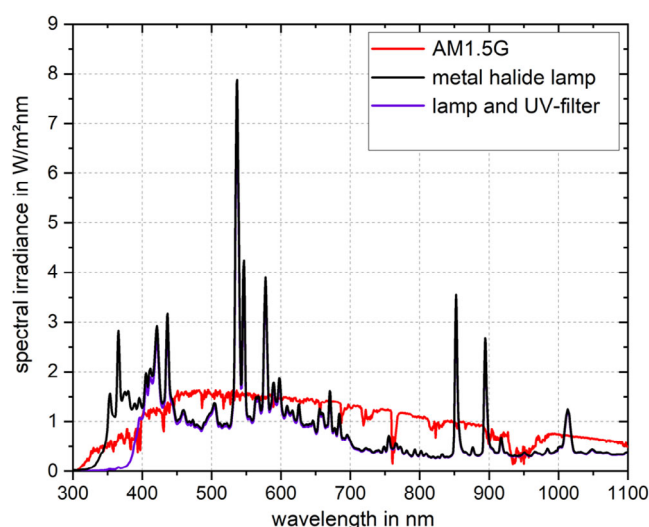


Figure 2. Spectrum of the metal halide lamp and the lamp plus UV-filter compared to AM1.5 G.

Table 2. The system in numbers.

Property	Type or range
Light source	Metal halide
Lamp control	Active
Light modes	Constant or cycled (shutter operation, per sample box)
Shutter slots	2
Light intensity	1–2 suns (applies to all boxes)
UV Filter	Optional
Temperature control	Active with Peltier elements, per sample box
Temperature range	-10 to $+100$ °C
Temperature modes	Constant or cycled
Sample boxes	8
Devices per sample box	8
Solar cells per device	6
Total number of solar cells	384
Tracking	Parallel for all cells
Tracking modes	MPPT, V_{oc} , J_{sc} , constant voltage (within photovoltage)
Variation of measurement modes	For every 4/8 devices of a sample box, a different tracking mode can be chosen
J – V scans	Sequentially
Atmosphere control	N_2 , air, dry air, others possible; per sample box

3. MPPT Electronics

The “micro” maximum power point tracking (μ MPPT) electronics are capable of continuous MPPT and can monitor a large number of solar cells individually. Additionally, they feature

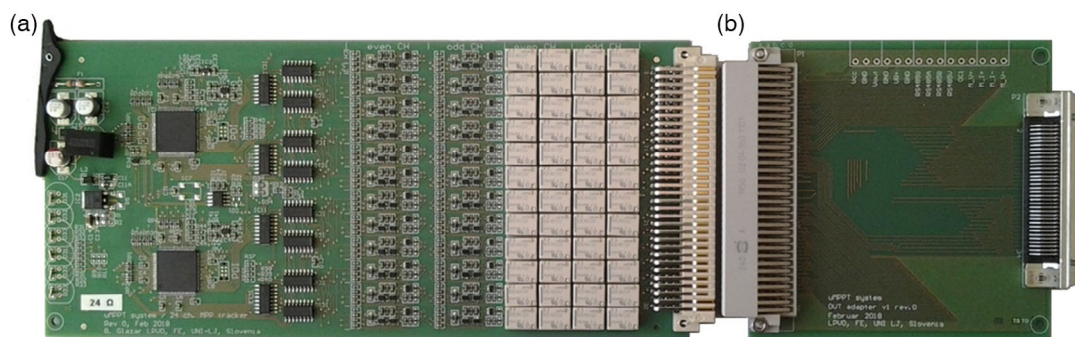


Figure 3. a) 24-channel μ MPPT board, b) DUT adapter board.

periodical switching to the measurement bus to connect individual cells to an external source-measurement unit for precise J – V scanning or additional analyses. The prefix “ μ ” refers to small area lab-scale solar cells.

The system consists of several micro μ MPPT cards (see **Figure 3**) that are inserted into a backplane of a sub-rack, which provides all the necessary interconnections. The μ MPPT cards are accessible from the backside through device-under-test (DUT) adapters, which are rerouting the measurement connections to adapt to the required wiring and cable arrangement. A single standard sub-rack can hold up to 12 μ MPPT cards. One μ MPPT card has 24 channels and can thus MPP-track 24 individual solar cells. Multiple crates can be connected to increase the number of channels. In the current version of the aging system, two sub-racks are utilized with 16 μ MPPT cards and 384 channels. The basic system architecture is shown in **Figure 4**.

Each channel consists of an electronic load, controlled by a microcontroller with voltage and current measurement capabilities, and is connected to the individual measured solar cell via a four-wire connection. Additionally, it is connected to the common measurement bus via relays (bypass). During the bypass of one chosen channel, all other cells remain in their selected mode of operation without interruption. The simplified schematics of the electronic load are shown in **Figure 5**.

The electronic load allows the connection of either single junction or tandem solar cells, such as silicon/perovskite photovoltaic (PV) cells. Therefore, the input voltage range is ± 1.65 V with automatic polarity detection to allow the operation of cells of both polarities on the same substrate. For cells with higher open-circuit voltage, the voltage range can be optionally extended to up to 2 V for one polarity by increasing the supply voltage while maintaining common reference voltage (COM).

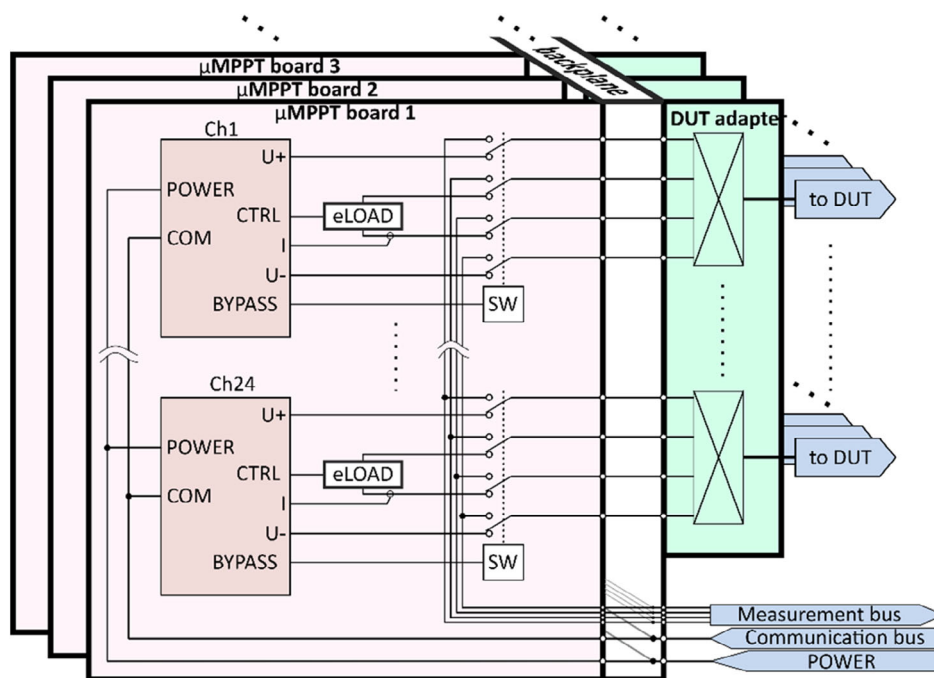


Figure 4. The μ MPPT system consists of 24-channel μ MPPT cards, inserted into a backplane with device-under-test (DUT) adapters allowing for flexible routing schemes.

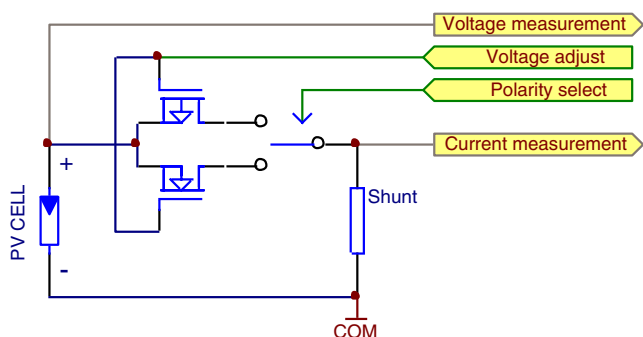


Figure 5. Simplified schematics of the electronic load stage of the μ MPPT.

As load, we chose metal–oxide–semiconductor transistors over the source-measurement approach, where operational power amplifiers are usually used. This maximizes efficiency, simplicity, integration, and significantly lowers the overall cost. However, the MPP-tracker cannot source power in this configuration but can only operate as a load. The load transistor is connected as a source follower, where the solar cell voltage follows gate voltage, making control simple and inherently stable. The measured solar cell's voltage is used as an input for the voltage regulation to compensate for the gate-source voltage difference. To allow dual polarity operation, two transistors are used. Two more transistors are added to select the correct polarity, shown as a switch in Figure 5. The input current range can be adjusted by choosing an appropriate current shunt resistor and can reach up to 50 mA, limited by the maximal power dissipation on load transistors.

A single microcontroller controls multiple channels. Internal analog-to-digital converters with differential inputs measure the solar cell's voltage and current. To accept both polarities, the common terminal of the cells is connected to a potential between the two supply rails of the microcontroller. This node is marked as COM in Figure 5. For noise reduction and increased resolution, digital averaging is performed at the interval of 200 ms to reduce the power-line interference for both 50 and 60 Hz environments. All channels are processed simultaneously in parallel; therefore, the measurement data of all channels is available every 200 ms.

A perturb and observe (P&O) algorithm^[36] (see Figure 6) is implemented in the microcontroller's firmware and runs independently of computer control. Based on the previous step, voltage is changed stepwise towards an expected higher power. The MPPT algorithm has an adjustable voltage step size and tracking step duration. The tracking step duration is input as a multiple of 200 ms, a fixed interval over which the cell's current is averaged. Within one tracking step, the power output of the last of the 200 ms measurement intervals is decisive for the direction of the following voltage change. The voltage step size stays fixed throughout an experiment. Tracking efficiency was determined to be 99.95%.^[37] A selectable voltage step size and tracking duration are essential to adapt to different PV cell technologies. For example, perovskite-based solar cells can exhibit large capacitance and hysteresis^[38] that can cause tracking problems.^[39] In the presented aging setup, a voltage step size of 0.01 V with a tracking step duration of 1 s is utilized typically. Besides the MPPT mode, open circuit, short circuit, and constant voltage modes can be selected independently for each channel. The microcontroller's firmware can be upgraded in place to provide easy updates of the algorithm.

4. Data Management and Track Selection

With two measurement parameters for MPPT and 12 for J - V scans (see Table S3, Supporting Information, for a complete overview) recorded over time for every single of the 384 solar cells, it becomes evident that the data management is challenging. The system records those values for each experiment separately, which is the run of one box. A particular challenge is to organize and categorize the data. Every substrate/device carries six individual solar cells. Our standard practice is to always age two devices of the same kind in one run to have good statistics. Those are averaged together, and for this reason, we define a cell parameter that tells the scripts that these devices are equal. The data management is realized in MATLAB, and plotting is performed semi-automatically.

Since the reproducibility of PSCs is still low,^[30] this is also reflected in the aging curves. MPP-tracks tend to have strange shapes, are unexpectedly low or unrealistically high, or cells just not get measured. The reasons for this can be manifold: While

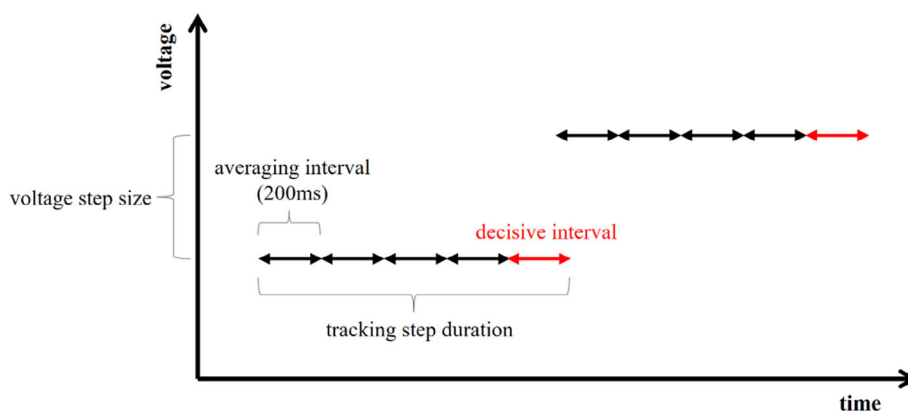


Figure 6. Schematic of the Perturb and Observe MPPT algorithm.

we assume that the inhomogeneity of the cells themselves is the main reason for this variety in aging behavior, it can also not be assured that all the 1024 contacting pins (64 devices contacted with eight double-pin contacts, see Figure S1, Supporting Information, for contact layout), are always reliable. Therefore, to discover trends in an aging experiment, it is necessary to pre-select the tracks that become analyzed. We are aware that selecting data is not known to be perfect scientific practice. However, we consider the unusual tracks erroneous or inaccurate and they should therefore be removed from the analysis. If peculiarities in the aging behavior or diverging trends are observed on a significant number of equal cells, this is still accounted for in the interpretation of data. Furthermore, we are constantly reporting how many cells of a particular cell stack are being analyzed, which is essential information on the reliability of the data. The selection rule is simple: All cells that behave similarly without significant irregularities will go into the analysis. There are two problems with this kind of analysis: It is not always given that all solar cells of two or more equivalent devices behave equivalent – then the behavior is chosen, which is seen for most solar cells. The other problem is that there is always room for human interpretation in the selection process, which is unavoidable. The burden of selecting in a fair and unbiased manner remains on the data analyst and is always followed with great care in our case.

Figure 7 gives an example of the selection process. The MPP tracks of all solar cells of two equivalent devices are plotted together in **Figure 7a**. There was a problem with device 8 cell 1 since the efficiency is below 1%, while other solar cells start the tracking above 18% PCE. Consequently, this cell is not used in further analysis. The data of device 8 cell 4 is very messy, pointing at a contact problem. The aging behavior of device 8 cell 4 and device 7 cell 4 is similar ascendingly. However, most cells behave differently. Therefore, those cells are also filtered out. While the initial general behavior of device 8 cells 3 and 5 is like the other cells' behavior, the tracks' overall height is significantly lower, and they are filtered out. Additionally, the aging behavior of device 8 cells 3 changes drastically after ≈ 230 h of aging, further justifying to filter the two cells starting lower in PCE. **Figure 7b** shows the MPP tracks that are considered valid and that are used for further analysis: To calculate average values or T_{80} . **Figure 7c** shows the average calculated from **Figure 7b** and the standard deviation displayed as an error bar. The spikes occurring every 24 h are artifacts of periodically performed $J-V$ scans. They appear on some types of solar cells and others not. This is believed to originate in different transient response times of different stacks, which causes hysteresis in $J-V$ scans depending on the scan speed.^[40,41] This is also why MPPT has become the standard method of determining PSC's stabilized efficiency.^[42]

5. Example Plots

Figure 8 shows different examples of plots that are generated automatically. Here, they only serve the purpose of display; the examples are not related. **Figure 8a** shows the average PCE from MPPT over aging time; the error bar represents the standard deviation. This is the most used plot since MPPT is

the strength of this aging system. **Figure 8b,c** shows the $J-V$ scans of one solar cell plotted together; the color code represents the aging time. **Figure 8c** shows the typical solar cell parameters PCE, V_{oc} , J_{sc} , and FF derived from daily $J-V$ scans in an aging experiment for forward and reverse scans of all solar cells of one device.

6. Challenges when Building the High-Throughput Aging System

In the following paragraph, we discuss challenges that arose during the development of the aging system.

A particular challenge when building a high-throughput aging system is to host and measure a large number of devices in a confined space. The larger the area that needs to be illuminated, the higher the cost of the lamp and the more difficult to maintain a good spatial homogeneity of the light. Therefore, the sample boxes need to be designed as small as possible, which leads to the next challenge: The packing density of the necessary contacting cables is already too high to be realized with cables but requires the design of a PCB, which hosts the contacting pins. This makes the contacting of devices limited to one particular layout of devices, which leads to the next problem: To test the electronics, the making of tester devices became necessary. Since a system can't be tested with an unstable testing device, small silicon photodiodes were mounted to a particularly designed PCB, which can be inserted into the sample boxes (see **Figure 9**). The used photodiodes are given in Table S4, Supporting Information.

As already mentioned in Section 2, the thermal coupling of the devices to the active temperature control requires a combination of unusual material properties: Thermal conductivity, electrical insulation, chemical inertness, non-stickiness, and elastic/soft material. Additionally, it has to stand a relatively wide temperature range of -10 to 100 °C. Finding the right material combination required a lot of testing, therefore we are providing the found material combination of a thermal interface material pad and glass-PTFE tape in Table S4, Supporting Information. It is important to mention that the thermal interface material should consist of non-silicon material, otherwise silicon oil can leave the heat pad and contaminate the samples. **Figure 10** shows details of the sample stages as well as the thermal interface pad.

Another difficulty concerning the devices has been to hold them down in position. A metal frame is used to press them down onto the heat-conducting pad and into the contacting pins. In the first version, this metal plate also had an opening to realize a lateral fixation. However, this turned out to regularly break the devices when a device got canted in the opening. A better solution was to remove the opening and press down the devices with a flat fixation plate (see **Figure S3**, Supporting Information). The lateral fixation of devices was then realized with pins that sit beside the devices (see **Figure 10d**).

The definitions of "inverted" and "regular" PSC devices do not necessarily correlate with the polarity of the contacts of devices, which lead to difficulties during the initial testing phase of the system. Therefore, we provide a short discussion of those in Supporting Information.

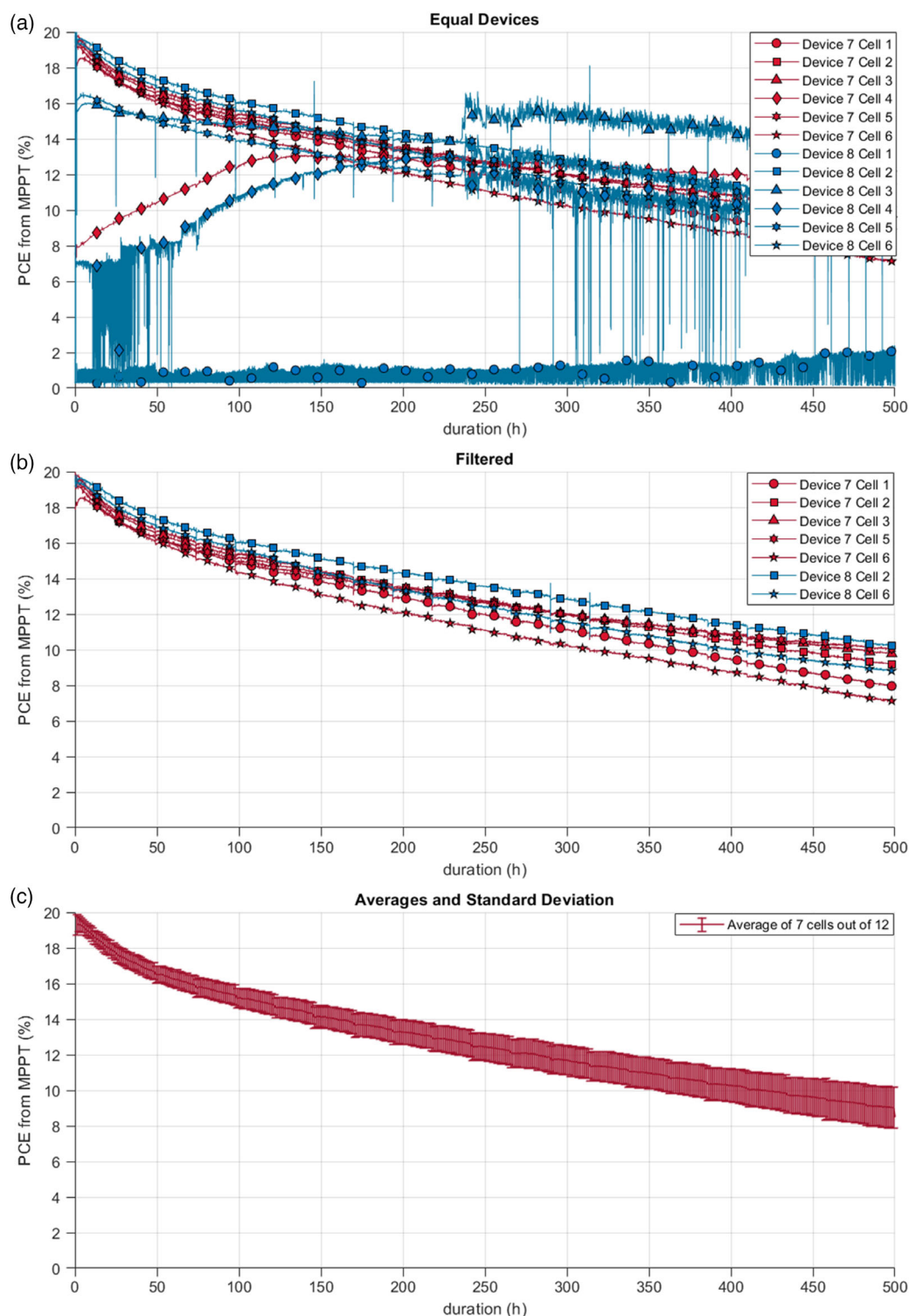


Figure 7. Example of the data selection process. a) Shows the raw data, b) shows MPP selected tracks, and c) shows the resulting average. The error bar represents the standard deviation.

A particular challenge during the design phase was to construct the sample boxes airtight. Especially the commercially available plugs to route the solar cells' currents and voltage

signals to the MPP electronics are not made to be impermeable. They were sealed by pouring a resin into the backside of the plugs. Another challenge was to design the lids of the sample

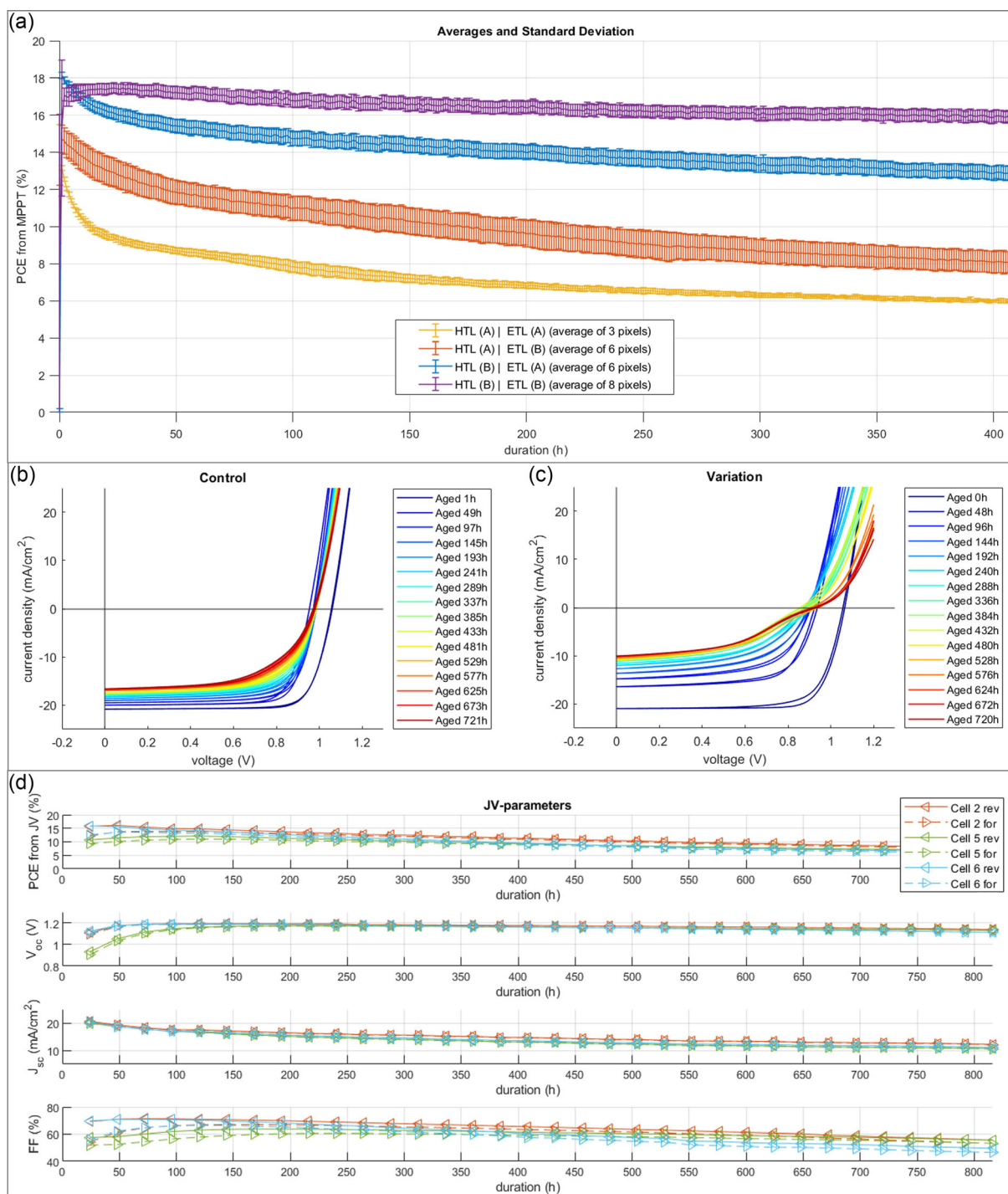


Figure 8. Example plots generated automatically.

boxes. The lids have to be transparent, which implies the use of glass, but they also need to be pressed down sufficiently against the gasket to properly close the box. Currently, a sheet of glass is glued into a metal frame. Then this frame can be screwed down, pressing the glass sheet into a silicone gasket. Under a constant flow of nitrogen, a humidity measurement showed a stable

humidity value of 0.1% RH, which is the lower limit of the measurement device used. Thus, the sample boxes are considered to be sufficiently airtight and provide an inert testing atmosphere.

Lastly, the water-cooling system which supplies cooled water into the sample boxes as a heatsink for the Peltier element, did show signs of electrochemical corrosion in the beginning. The

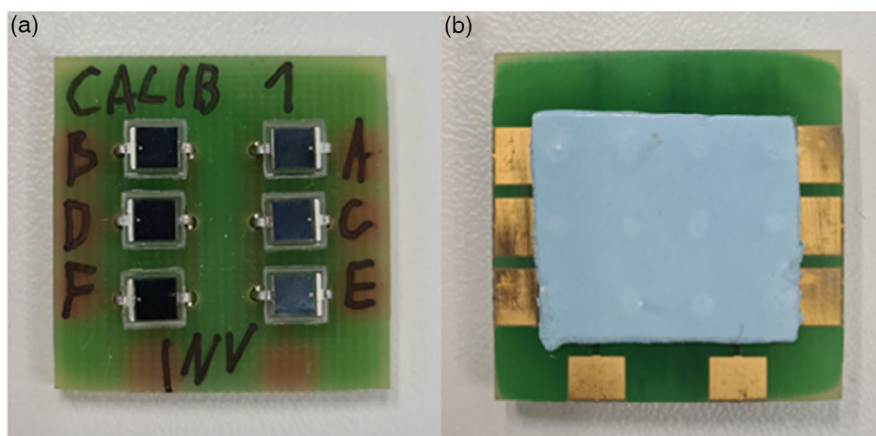


Figure 9. Devices made to test the system. Printed circuit board (PCB) size is 2.5×2.5 cm. a) shows the front side with the photodiodes facing the illumination source. Each photodiode represents a solar cell on the actual perovskite solar cell (PSC) devices. b) shows the backside with gold contacts that match the contacting layout of the system. A blue thermal isolation pad covers the through-hole contacts of the diodes to avoid shunting on the copper block of a sample box.

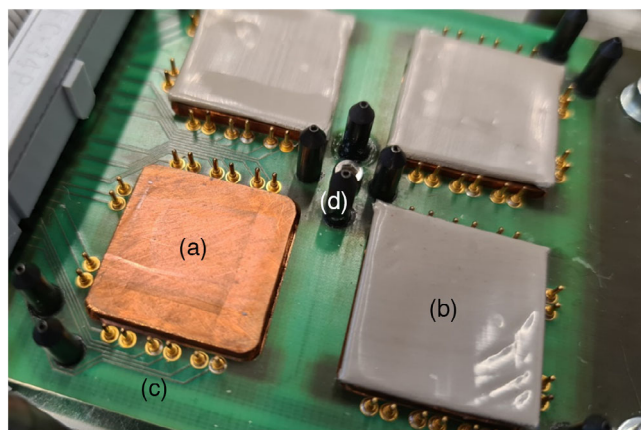


Figure 10. Four sample stages. a) Copper block connected to the Peltier element. All four sample stages shown are connected to the same Peltier element. b) Combination of a thermal interface material pad wrapped in PTFE tape for direct contact with the active area of samples. c) Contacting pins for electrical connection of devices. Two pins are contacting one contact of the solar cell for 4-wire measurements. d) Pins that define the lateral position of a device.

problem was solved by replacing all metal parts within the water cycle with stainless steel. Before, brass adapters and aluminum tubes were used in some places.

7. Considerations on Improvements

The following paragraph discusses what we would improve if we built another high-throughput aging system based on the lessons learned for this system. One major problem has been the gas-tightness of the sample boxes, as discussed in the previous section. Therefore, including humidity and oxygen sensors into the sample boxes is an important improvement we'd implement. The temperature can only be set for an entire box in the current

system version. However, since temperature variations are interesting with respect to accelerated ageing,^[43] it would be a considerable improvement to allow for two different temperatures within one box, one temperature for four devices.

8. Requirements for Collaboration

We are happy to receive devices to be tested. The easiest way is to use the suitable dimensions and contact layout for devices shown in Figure S1, Supporting Information. Since this will not always be feasible for users, we are also able to receive devices with open contacts in a limited capacity. Currently, users can apply for access to the high-throughput aging system in the VIPERLAB project.^[44]

9. Conclusion

This research instrument paper presented details of a high-throughput aging system for parallel MPPT of PSCs. We gave information on the system's capabilities and the development process as well as valuable details for engineers, who would want to design a similar system. Table 2 provides an overview of the essential properties of the high-throughput aging system.

Supporting Information

Supporting Information is available from the Wiley Online Library or from the author.

Acknowledgements

H.K. would like to thank Thomas Lußky, Hagen Heinz, Carola Ferber, and Monika Gabernig for the technical support at HZB. The authors acknowledge Tobias Hänel for measuring the lamp spectrum and Rayk Horn for support with soldering PCBs. H.K. would like to thank Hampus Nasström and Dr. Aboma Merdasa for their support with MATLAB scripting.

H.K. acknowledges the support from the HyPerCells graduate school. M.J., B.G. and M.T. thank the Slovene Research Agency (ARRS) for funding through the research program P2-0415.

Open Access funding enabled and organized by Projekt DEAL.

Conflict of Interest

The authors declare no conflict of interest.

Data Availability Statement

The data that support the findings of this study are available on request from the corresponding author. The data are not publicly available due to privacy or ethical restrictions.

Keywords

aging, MPP-tracking, MPPT, perovskite solar cells, stability testing

Received: March 15, 2022

Published online:

- [1] Best Research-Cell Efficiency Chart, Photovoltaic Research, NREL <https://www.nrel.gov/pv/cell-efficiency.html>, (accessed: March 2022).
- [2] C. C. Boyd, R. Cheacharoen, T. Leijtens, M. D. McGehee, *Chem. Rev.* **2019**, *119*, 3418.
- [3] R. Wang, M. Mujahid, Y. Duan, Z. K. Wang, J. Xue, Y. Yang, *Adv. Funct. Mater.* **2019**, *29*, 1808843.
- [4] S. S. Dipta, A. Uddin, *Energy Technol.* **2021**, *9*, 2100560.
- [5] R. Cheacharoen, C. C. Boyd, G. F. Burkhard, T. Leijtens, J. A. Raiford, K. A. Bush, S. F. Bent, M. D. McGehee, *Sustain. Energy Fuels* **2018**, *2*, 2398.
- [6] S. Ma, Y. Bai, H. Wang, H. Zai, J. Wu, L. Li, S. Xiang, N. Liu, L. Liu, C. Zhu, G. Liu, X. Niu, H. Chen, H. Zhou, Y. Li, Q. Chen, *Adv. Energy Mater.* **2020**, *10*, 1902472.
- [7] Y. Il Lee, C. Lee, *Adv. Energy Mater.* **2018**, *8*, 1701928.
- [8] F. Bella, G. Griffini, J. P. Correa-Baena, G. Saracco, M. Grätzel, A. Hagfeldt, S. Turri, C. Gerbaldi, *Science* **2016**, *354*, 203.
- [9] T. Leijtens, G. E. Eperon, S. Pathak, A. Abate, M. M. Lee, H. J. Snaith, *Nat. Commun.* **2013**, *4*, 2885.
- [10] M. V. Khenkin, et al., *Nat. Energy* **2020**, *5*, 35.
- [11] N. Phung, M. Verheijen, A. Todorova, K. Datta, M. Verhage, A. Al-Ashouri, H. Köbler, X. Li, A. Abate, S. Albrecht, M. Creatore, *ACS Appl. Mater. Interfaces* **2022**, *14*, 2166.
- [12] L. Canil, J. Salunke, Q. Wang, M. Liu, H. Köbler, M. Flatken, L. Gregori, D. Meggiolaro, D. Ricciarelli, F. De Angelis, M. Stollerfoht, D. Neher, A. Priimagi, P. Vivo, A. Abate, *Adv. Energy Mater.* **2021**, *11*, 2101553.
- [13] M. Roß, S. Severin, M. B. Stutz, P. Wagner, H. Köbler, M. Favini-Lévêque, A. Al-Ashouri, P. Korb, P. Tockhorn, A. Abate, B. Stannowski, B. Rech, S. Albrecht, *Adv. Energy Mater.* **2021**, *11*, 2101460.
- [14] P. Caprioglio, D. S. Cruz, S. Caicedo-D'vila, F. Zu, A. A. Sutanto, F. Peña-Camargo, L. Kegelmann, D. Meggiolaro, L. Gregori, C. M. Wolff, B. Stiller, L. Perdigon-Toro, H. Köbler, B. Li, E. Gutierrez-Partida, I. Lauermaun, A. Abate, N. Koch, F. De Angelis, B. Rech, G. Grancini, D. Abou-Ras, M. K. Nazeeruddin, M. Stollerfoht, S. Albrecht, M. Antonietti, D. Neher, *Energy Environ. Sci.* **2021**, *14*, 4508.
- [15] E. Aktas, N. Phung, H. Köbler, D. A. González, M. Méndez, I. Kafedjiska, S.-H. Turren-Cruz, R. Wenisch, I. Lauermaun, A. Abate, E. Palomares, *Energy Environ. Sci.* **2021**, *14*, 3976.
- [16] O. Bettucci, J. Pascual, S. H. Turren-Cruz, A. Cabrera-Espinoza, W. Matsuda, S. F. Völker, H. Köbler, I. Nierengarten, G. Reginato, S. Collavini, S. Seki, J. F. Nierengarten, A. Abate, J. L. Delgado, *Chem.* **2021**, *27*, 8110.
- [17] J. Dagar, M. Fenske, A. Al-Ashouri, C. Schultz, B. Li, H. Köbler, R. Munir, G. Parmasivam, J. Li, I. Levine, A. Merdasa, L. Kegelmann, H. Näsström, J. A. Marquez, T. Unold, D. M. Többsens, R. Schlatmann, B. Stegemann, A. Abate, S. Albrecht, E. Unger, *ACS Appl. Mater. Interfaces* **2021**, *13*, 13022.
- [18] J. Li, J. Dagar, O. Shargaieva, M. A. Flatken, H. Köbler, M. Fenske, C. Schultz, B. Stegemann, J. Just, D. M. Többsens, A. Abate, R. Munir, E. Unger, *Adv. Energy Mater.* **2021**, *11*, 2003460.
- [19] J. Hidalgo, C. A. R. Perini, A. F. Castro-Mendez, D. Jones, H. Köbler, B. Lai, R. Li, S. Sun, A. Abate, J. P. Correa-Baena, *ACS Energy Lett.* **2020**, *5*, 3526.
- [20] M. Kot, L. Kegelmann, H. Köbler, M. Vorokhta, C. Escudero, P. Kúš, B. Šmíd, M. Tallarida, S. Albrecht, A. Abate, I. Matolínová, D. Schmeißer, J. I. Flege, *ChemSusChem* **2020**, *13*, 5722.
- [21] D. Di Girolamo, N. Phung, F. U. Kosasih, F. Di Giacomo, F. Matteocci, J. A. Smith, M. A. Flatken, H. Köbler, S. H. Turren Cruz, A. Mattoni, L. Cinà, B. Rech, A. Latini, G. Divitini, C. Ducati, A. Di Carlo, D. Dini, A. Abate, *Adv. Energy Mater.* **2020**, *10*, 2000310.
- [22] Q. Wang, J. A. Smith, D. Skroblin, J. A. Steele, C. M. Wolff, P. Caprioglio, M. Stollerfoht, H. Köbler, M. Li, S. H. Turren-Cruz, C. Gollwitzer, D. Neher, A. Abate, *Sol. RRL* **2020**, *4*, 2000213.
- [23] N. Phung, R. Félix, D. Meggiolaro, A. Al-Ashouri, G. Sousa e Silva, C. Hartmann, J. Hidalgo, H. Köbler, E. Mosconi, B. Lai, R. Gunder, M. Li, K.-L. Wang, Z.-K. Wang, K. Nie, E. Handick, R. G. Wilks, J. A. Marquez, B. Rech, T. Unold, J.-P. Correa-Baena, S. Albrecht, F. De Angelis, M. Bär, A. Abate, *J. Am. Chem. Soc.* **2020**, *142*, 2364.
- [24] Y. Lin, B. Chen, Y. Fang, J. Zhao, C. Bao, Z. Yu, Y. Deng, P. N. Rudd, Y. Yan, Y. Yuan, J. Huang, *Nat. Commun.* **2018**, *9*, 4981.
- [25] K. Domanski, E. A. Alharbi, A. Hagfeldt, M. Grätzel, W. Tress, *Nat. Energy* **2018**, *3*, 61.
- [26] M. V. Khenkin, K. M. Anoop, I. Visoly-Fisher, F. Di Giacomo, I. Dogan, B. R. Patil, V. Turkovic, M. Madsen, Y. Galagan, C. Ulbrich, E. A. Katz, in *Conf. Rec. IEEE Photovolt. Spec. Conf.*, IEEE, Piscataway, NJ **2020**, pp. 0305–0308.
- [27] M. V. Khenkin, K. M. Anoop, E. Katz, I. Visoly-Fisher, *Energy Environ. Sci.* **2019**, *12*, 550.
- [28] M. Li, C. Zuo, J. Hu, L. Ding, *Sci. Bull.* **2021**, *66*, 1372.
- [29] M. Stollerfoht, C. M. Wolff, Y. Amir, A. Paulke, L. Perdigon-Toro, P. Caprioglio, D. Neher, *Energy Environ. Sci.* **2017**, *10*, 1530.
- [30] M. L. Petrus, J. Schlipf, C. Li, T. P. Gujar, N. Giesbrecht, P. Müller-Buschbaum, M. Thelakkat, T. Bein, S. Hüttner, P. Docampo, *Adv. Energy Mater.* **2017**, *7*, 1700264.
- [31] F. Li, M. Liu, *J. Mater. Chem. A* **2017**, *5*, 15447.
- [32] L. Shi, M. P. Bucknall, T. L. Young, M. Zhang, L. Hu, J. Bing, D. S. Lee, J. Kim, T. Wu, N. Takamure, D. R. McKenzie, S. Huang, M. A. Green, A. W. Y. Ho-Baillie, *Science* **2020**, *368*, 1.
- [33] M. V. Khenkin, A. K. M., I. Visoly-Fisher, S. Kolusheva, Y. Galagan, F. Di Giacomo, O. Vukovic, B. R. Patil, G. Sherafatipour, V. Turkovic, H.-G. Rubahn, M. Madsen, A. V. Mazanik, E. A. Katz, *ACS Appl. Energy Mater.* **2018**, *1*, 799.
- [34] L. Jiang, J. Lu, S. R. Raga, J. Sun, X. Lin, W. Huang, F. Huang, U. Bach, Y. B. Cheng, *Nano Energy* **2019**, *58*, 687.
- [35] F. Huang, L. Jiang, A. R. Pascoe, Y. Yan, U. Bach, L. Spiccia, Y. B. Cheng, *Nano Energy* **2016**, *27*, 509.

- [36] L. Rakocevic, F. Ernst, N. T. Yimga, S. Vashishtha, T. Aernouts, T. Heumueller, C. J. Brabec, R. Gehlhaar, J. Poortmans, *Sol. RRL* **2019**, 3, 1800287.
- [37] B. Glazar, G. Matič, M. Jošt, M. Topič, in *37th Eur. Photovolt. Sol. Energy Conf.* **2020**, pp. 653–656 <https://doi.org/10.4229/EUPVSEC20202020-3BV.1.14>.
- [38] B. Chen, M. Yang, S. Priya, K. Zhu, *J. Phys. Chem. Lett.* **2016**, 7, 905.
- [39] N. Pellet, F. Giordano, M. Ibrahim Dar, G. Gregori, S.M. Zakeeruddin, J. Maier, M. Grätzel, *Prog. Photovoltaics Res. Appl.* **2017**, 25, 942.
- [40] T. Song, D.J. Friedman, N. Kopidakis, *Sol. RRL* **2022**, 6, 2100867.
- [41] L. Kegelmann, C. M. Wolff, C. Awino, F. Lang, E. L. Unger, L. Korte, T. Dittrich, D. Neher, B. Rech, S. Albrecht, *ACS Appl. Mater. Interfaces* **2017**, 9, 17245.
- [42] R.B. Dunbar, B.C. Duck, T. Moriarty, K.F. Anderson, N.W. Duffy, C.J. Fell, J. Kim, A. Ho-Baillie, D. Vak, T. Duong, Y. Wu, K. Weber, A. Pascoe, Y.B. Cheng, Q. Lin, P.L. Burn, R. Bhattacharjee, H. Wang, G.J. Wilson, *J. Mater. Chem. A* **2017**, 5, 22542.
- [43] F. Schenkelberg, *Reliability Characterisation Of Electrical And Electronic Systems* (Ed: J.) Swingler), Woodhead Publishing, Swaston, UK **2015**, pp. 215–250.
- [44] VIPERLAB - *Fully Connected Virtual and Physical Perovskite Photovoltaics Lab*. <https://www.viperlab.eu/> (accessed: December 2021).